Smart Structures and Systems, *Vol. 32, No. 4 (2023) 195-205*
https://doi.org/10.12989/sss.2023.32.4.195

Acoustic emission localization in concrete using a wireless air-coupled monitoring system

Yunshan Bai [1,2a], Yuanxue Liu[*1], Guangjian Gao [2] and Shuang Su [2]

[1] *Chongqing Key Laboratory of Geomechanics & Geoenvironmental Protection, Department of Military Installations, Army Logistics Academy of PLA, Chongqing 401311, Republic of China*
[2] *Department Basic Department, Army Logistics Academy of PLA, Chongqing 401311, Republic of China*

(*Received March 10, 2022, Revised January 16, 2023, Accepted March 16, 2023*)

Abstract. The contact acoustic emission (AE) monitoring system is time-consuming and costly for monitoring concrete structures in large scope, in addition, the great difference in acoustic impedance between air and concrete makes the detection process inconvenient. In this work, we broaden the conventional AE source localization method for concrete to the non-contact (air-coupled) micro-electromechanical system (MEMS) microphones array, which collects the energy-rich leaky Rayleigh waves, instead of the relatively weak P-wave. Finite element method was used for the numerical simulations, it is shown that the propagation velocity of leaky Rayleigh waves traveling along the air-concrete interface agrees with the corresponding theoretical properties of Lamb wave modes in an infinite concrete slab. This structures the basis for implementing a non-contact AE source location approach. Based on the experience gained from numerical studies, experimental studies on the proposed air-coupled AE source location in concrete slabs are carried out. Finally, it is shown that the locating map of AE source can be determined using the proposed system, and the accuracy is sufficient for most field monitoring applications on large plate-like concrete structures, such as tunnel lining and bridge deck.

Keywords: acoustic emission; air-coupled; beamforming; concrete structures; leaky Rayleigh wave; location; monitoring system

1. Introduction

When the civil engineering structures crack under stress, strain energy is released in the form of transient stress waves. By analyzing these stress wave signals, various information of damage source can be obtained, including damage location, damage type, material characteristics and so on, which is called acoustic emission technique (AET). It is a sensitive passive monitoring technique that has been widely used in defect location research in the field of civil engineering health monitoring (Li *et al*. 2017, Banjara *et al*. 2019, Du *et al*. 2021). From the energy point of view (Carpinteri *et al*. 2016), AE is the emission of a surplus of elastic energy under loading, which is not dissipated by the material damage (such as the opening and closing of micro-cracks), and is detected by the AE sensors. Therefore, the remarkable feature of AE technique is that it only detects active cracks, and it cannot detect inactive cracks or damages that do not emit energy outward. There are many kinds of damages in materials, for the damages that do not emit energy, the energy balance may be reached itself, which does not affect the stability of the whole structure.

AE source is the location of damage, the positioning of the AE sources is an important aspect of structural health monitoring research (Kuang *et al*. 2016). At present, the piezoelectric sensor is mainly used for acoustic emission monitoring, these sensors need to be strongly bonded on the surface of the detected structure during the whole monitoring process. Another problem with current sensor monitoring is the need for wired data acquisition equipment, it is time-consuming and laborious to place a large number of sensors to monitor larger range. For conventional AE systems, they are capable of recording AE signals in the MHz range that are ideal for monitoring microcrack evolution in the laboratory (Shahidan *et al*. 2013). The cost of the complete set of equipment is about USD $40,000-60,000, which is costly and bulky to be used for monitoring a large structure. Therefore, they are not suitable for field monitoring of large civil engineering structures.

In recent years, the non-contact (air-coupled) NDT (non-destructive testing) methods have attracted widespread attention in the field of structural health monitoring (Chen *et al*. 2019). Non-contact wireless sensors and Internet of Things technology make it possible to monitor large-scale concrete structural. However, there are two challenges to study the non-contact (air coupled) AE location of concrete structures (Ferguson *et al*. 2002, Qiu and Lau 2021). One is the attenuation of high frequency stress wave signals by concrete, only AE signals at low frequencies (below 25 kHz) can propagate farther. Another is the huge difference in acoustic impedance between air and concrete, where only a small amount of energy leaks into the air near the

*Corresponding author, Professor,
E-mail: lyuanxue@vip.sina.com
[a] Ph.D., E-mail: yunshanbai@qq.com

ISSN: 1738-1584 (Print), 1738-1991 (Online)

interface (Ongpeng *et al*. 2018).

With the rapid development of electronic science and technology, air-coupled sensors are able to detect leaky surface waves and leaky Lamb waves (Qiu and Lau 2021). Therefore, considering the AE source can be located by monitoring the leaky surface wave on the concrete surface rather than direct acoustic waves in the air, it can make full use of the advantage of AE technique to detect active defects, and be conveniently applied to the damage monitoring of practical large-scale civil structures. The MEMS (micro-electromechanical system) microphones sensor (around USD $0.314) is far less expensive than a contact piezoelectric sensor, the small size and low unit cost enables deployment of many sensors in an array and monitoring system of large civil structure based on wireless connection. The multi-channel sensor array data will be processed using beamforming technique (Xiao *et al*. 2014). Beamforming is a signal processing technique, which is widely used in multi-channel signal processing (Mclaskey *et al*. 2010, Wang *et al*. 2020).

This paper focuses on two aspects: one is the characteristics of AE signals that leak from the concrete surface to the air, and the other is the response characteristics of non-contact (air-coupled) sensors to AE signals. An AE source location method is proposed by theoretical analysis and numerical calculation. Based on the above theoretical research results, a non-contact monitoring system based on the wireless connection of Raspberry Pi (single-board computer) is made to locate the AE source, and the effect of the location is verified experimentally. This research aims to develop an inexpensive non-contact technique to acquire accurate location of AE source on large plate-like concrete structures and prepare for the monitoring of large civil structures based on wireless Internet of Things.

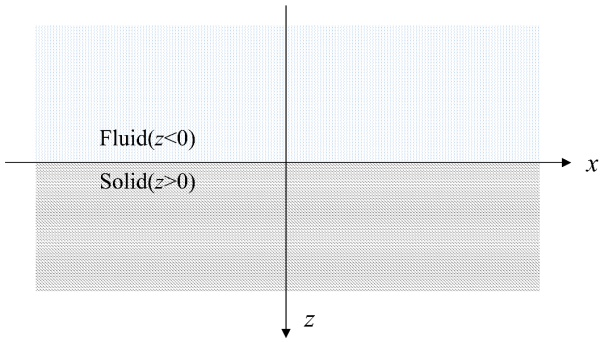

Fig. 1 A fluid-solid half space system

2. Waveguide modes in an air/concrete plate

For a fluid-solid half space system, as depicted in Fig. 1, the fluid ($z < 0$) is above the solid. Material parameters of fluid are given by the Lame's constant λ_f and ρ_f, and those of the solid by the Lame's constant λ_s, μ and density ρ_s. The governing equations of fluid-solid half space are derived from the displacement potential function φ in the fluid and solid, which are given in Eq. (1)

$$\frac{\partial^2 \varphi_i}{\partial x^2} + \frac{1}{x}\frac{\partial \varphi_i}{\partial x} + \frac{\partial^2 \varphi_i}{\partial z^2} - \frac{\varphi_i}{x^2} = \frac{1}{c_S^2}\ddot{\varphi}_i \tag{1}$$

Where subscripted variable i includes F, P, and S, for the fluid $c_F^2 = \lambda_f/\rho_f$ is the acoustic velocity, for the solids $c_P^2 = (\lambda_s + 2\mu)/\rho_s, c_S^2 = \mu/\rho_s$ are P-wave velocity and S-wave velocity respectively. The double dots represent a double differentiation of time. In general, a free surface solid model (vacuum-solid half space) can correctly calculate the propagation of elastic waves in the solid interface because air has little effect on solids (Redwood 1967).

When stress waves from AE activity propagate in plate-like concrete structure, Rayleigh waves propagate at the solid interface. If the thickness of the plate is smaller than the wavelength of the guided wave, the Rayleigh waves will degenerate into Lamb waves (Aggelis and Matikas 2012), therefore, Rayleigh wave is a special type of guided wave, which propagates along the surface of a semi-infinite solid medium.

Fig. 2 presents the dispersion curve of a free surface

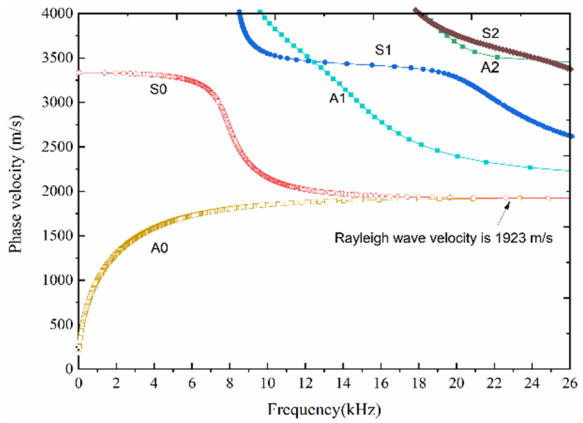

(a) Phase velocity dispersion curves

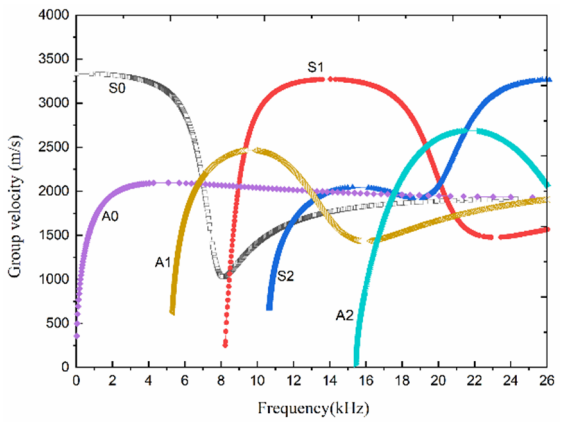

(b) Group velocity dispersion curves

Fig. 2 Dispersion curves of a free surface concrete slab (the thickness is 200 mm, density is 2400 kg/m^3, Young's modulus is 25.63 GPa and Poisson's ratio is 0.2)

concrete slab. At the lower frequency (< 7 kHz), only the modes A0 and S0 exist. At higher frequency, A0 and S0 modes will approach the Rayleigh wave velocity of the plate. Commonly, in this case, Rayleigh wave motion develops at a range of 12 to 14 kHz; this is where A0 and S0 modes combine together at the Rayleigh wave velocity. Rayleigh wave velocity, as determined for free solids (as shown in Fig. 2(a)), is a very good approximation of the surface wave phase velocity on air-concrete interfaces, this is because the density of solids is significantly greater than that of liquids (e.g., air density is 1.21 kg/m^3 and concrete density is 2400 kg/m^3) (Plona *et al*. 1975). The energy of the wave propagates in group velocity, which is equal to the phase velocity divided by the number of waves. The dispersion group velocity curve can be obtained as shown in Fig. 2(b).

In plate-like structures (e.g., tunnel lining and bridge deck), the AE signal stress wave propagates on the plate surface can be considered as plane wave, the small aperture arrays are more sensitive to changes in azimuth than changes in slowness (slowness of plane wave is approximately equal to 1/c, c is the propagation velocity), more details can be found in Mclaskey *et al*. (2010). Thus, for the AE source location of plate-like structure, it is equivalent to finding the arrival direction of AE wave in a two-dimensional plane.

In addition, leaky Rayleigh waves also show dispersion phenomenon during propagation. However, this dispersion differs from the Rayleigh waves in solids, which cause the variation of phase velocity with frequency. The velocity of Leaky Rayleigh waves propagation at the fluid/solid interface is constant (Kaczmarek *et al*. 2017), which provides convenience for beamforming localization of AE sources.

3. Data processing method

3.1 MASW analysis

The dispersion curve of plate structure can be obtained by MASW (multichannel analysis of surface waves) technique (Park *et al*. 1998), which is based on non-contact acoustic signal has great potential for characterizing the properties of plate-like concrete structure. In this paper, MASW technique is used to obtain the dispersion curve of concrete slab to be monitored, so as to obtain the parameters such as the velocity of leaky surface wave, and this result is compared with the theoretical dispersion curve based on Lamb wave theory.

Multiple leaky surface wave signals from AE sources are received through a linear array, the array data collected at different offsets u(x,t) is automatically transformed to the frequency-phase-velocity domain, the plane-wave transformation is given by

$$M(\omega, c_R) = \int e^{-i(\frac{\omega}{c_R})x} U(x, \omega) dx \tag{2}$$

where U(x,ω) is obtained from the Fourier transformation of u(x,t), ω is the angular frequency, c_R is the measured phase velocity, and M(ω,c_R) is the stack amplitude for each ω and c_R., M is calculated in the frequency and phase-velocity range of interest to generate the frequency-phase-velocity spectrum, and this spectrum shows how the total AE energy in concrete is distributed between different frequencies and phase velocities. In dispersion images, red represents high energy and blue represents low energy. As the frequency increases (between 12 kHz and 14 kHz), it can be seen that the energy of A0 and S0 modes combine at one velocity (the red is more and more concentrated), which is the velocity of leaky surface wave c_{LR}. Therefore, we first obtain dispersion images based on the multi-channel waveform signals obtained by monitoring, and then obtain the velocity of leaky surface wave c_{LR} based on the energy distribution (red area) on the figure.

3.2 Beamforming-based positioning method

The delay and sum beamforming method is used to process signals received by each single square array and form a beam. The basis of time delay beamforming is to calculate the relative delays from all locations on the surface of an AE source to each microphone in the array. The reconstruction function for the locations in the image plane is obtained by Xiao *et al*. (2014)

$$B(\vec{r}, t) = \frac{1}{N} \sum_{n=1}^{N} B_n (t - \Delta_n) \tag{3}$$

where $\vec{r}$ is the vector position of the point in the reconstruction plane, B_n is the recorded time signal of the nth microphone, and Δ_n is the relative delay. The relative delays are calculated from the absolute delays (τ_n) according to $\Delta_n = \tau_n - min(\tau_n)$. The absolute delays have the form $\tau_n = d_n / c_{LR}$, where c_{LR} is the leaky Rayleigh wave velocity, d_n is the vector distance between each microphone in the array and the points in the image plane, the leaky Rayleigh wave velocity c_{LR} is determined by the MASW analysis described in Section 3.1 above.

The leaky Rayleigh waves used for positioning in this paper are monitored on the surface close to the concrete, so the positioning of the AE source can be simplified to a two-dimensional planar positioning problem. The coordinate corresponding to the maximum amplitude in the intersection area is taken as the location of the AE source, this positioning process can be programmed automatically, and the detailed analysis process is shown in Fig. 3 below. In the numerical and experimental studies below, the AE sources are located at the intersection of two beams formed by a pair of square arrays, similar to human “ears”.

4. Numerical study

In this section, the numerical simulation data will be used to establish the air-coupled AE source location method, including air-coupled MASW and air-coupled beamforming. A two-dimensional (2D) axisymmetric finite element model and a three-dimensional (3D) finite element model are established respectively, the 2D simulations are

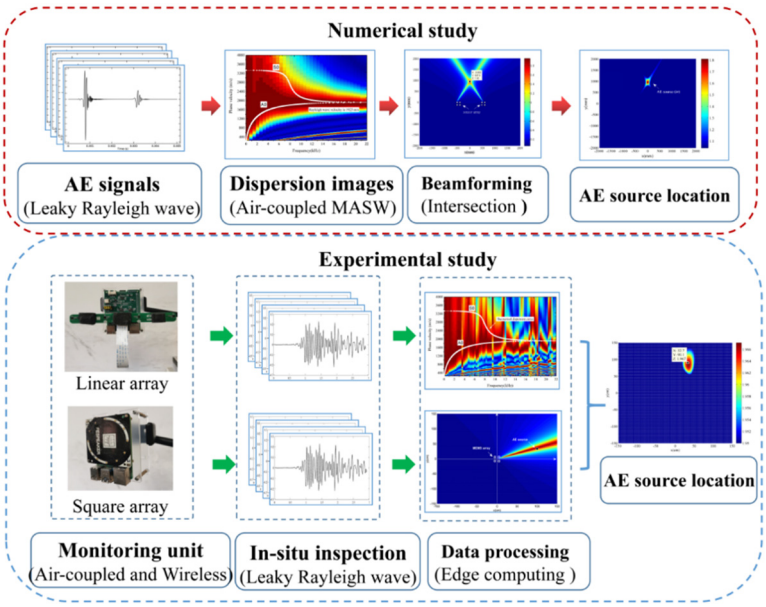

Fig. 3 Research methods and processes

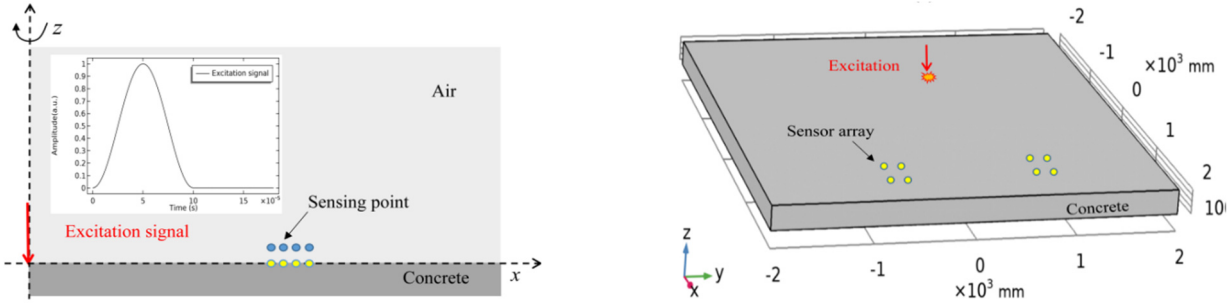

(a) 2D axisymmetric air-concrete model for MASW

(b) 3D concrete slab model for AE source location

Fig. 4 The finite element model

conducted to generate Leaky Rayleigh wave data from concrete surface with artificial AE source. the velocity of the leaky Rayleigh wave is obtained by MASW processing, then the Rayleigh waveforms are used to form the beam, and finally the location of the AE source is determined in a 3D finite element model.

4.1 Establishment of the finite element model

In order to observe the results of theoretical analysis, the numerical analysis for air-solid half space system was achieved using COMSOL, a software that implements the elastodynamic finite element method, which is based on the MATLAB environment.

As shown in Fig. 4(a), a simulated AE signal was loaded at the air-solid interface to simulate leaky Rayleigh wave propagation characteristics. The highly heterogeneous composition of concrete is a challenge for AE analysis, and in this study, the properties of each concrete are assumed to be homogeneous and linear-elastic. As the leaky surface waves at relatively low frequencies (10 kHz~22 kHz and wavelengths around 8~19 cm) are notably longer than the largest coarse aggregate. Since the Rayleigh wave on the concrete surface and the leaky Rayleigh wave in the air can be used for positioning (the specific reasons are analyzed in section 4.2.3 below), in order to save the cost of calculation, the 3D solid model without air domain, as shown in Fig. 4(b), is used to numerically calculated the beamforming positioning.

The material parameters used for numerical calculation are consistent with those of theoretical analysis, for air, density ρ_f is 1.21 kg/m^3, sound velocity c_F is 343 m/s; for concrete, density ρ_s is 2400 kg/m^3, P-wave velocity c_P = 3444 m/s, and Poisson's ratio ν is 0.2. The vertical transient point load is $f(t) = \sin^2(\pi t/T)$, the pulse width T is 100 μs, and the time step is 1μs. The size of the model is 4000 mm in horizontal x-axis and 1200 mm in the vertical z-axis, the model is large enough to avoid unnecessary boundary reflection.

For a maximum frequency f_{max} = 20 kHz, considering a S-wave velocity c_s = 2109 m/s, the speed of sound in air c_F = 343 m/s, in present study the minimum wavelength is given by $\lambda_{min} = c_i / f_{max}$ (i=S, F), for the 2D axisymmetric air-concrete model, the value of λ_{min} is assigned as 10 cm in solid and 2 cm in air. For the 3D concrete slab model, the value of λ_{min} is assigned as 10 cm.

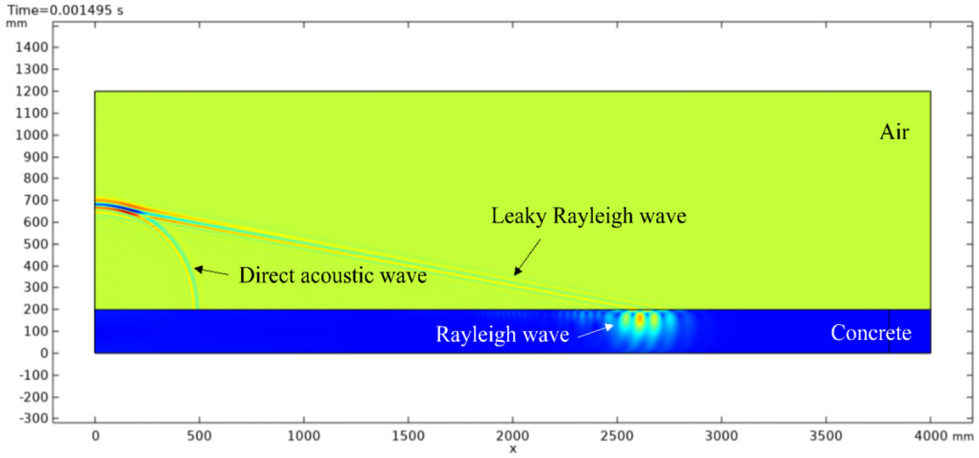

Fig. 5 Snapshot of pressure (in air) and stress (in concrete) after 0.001495 s from the excitation

To avoid numerical instability, the integration time step and the element size are dependent on the maximum frequency f_{max}. There is a super rule that a minimum of 20 points per cycle at the highest frequency, that is $\Delta t = 1 / (20 f_{max})$. For a good spatial resolution, 20 nodes per wavelength are normally required at least. Therefore, the element size is $l_e = \lambda_{min} / 20 = 5$ mm in solid and 1 mm in air. Both 2D and 3D models are solved with an integration time step $\Delta t = 1$ μs.

The corresponding sound pressure responses were collected by 4 sensing points with a spacing of 50 mm and 20 mm height from the concrete surface.

4.2 Numerical simulation of fluid-solid half space based on axisymmetric 2D model

4.2.1 Wave propagation at the air-concrete interface

According to the theoretical analysis, the vertical point load at the air-solid interface will excite many modes of guided waves in the solid, including P-wave, S-wave, Rayleigh wave, air acoustic wave and Scholte waves. Because Rayleigh waves have larger out-of-plane motion and attenuate slower with distance than body waves (i.e., P-wave and S-wave), leaky Rayleigh waves are more easily detected by air-coupled sensors.

Fig. 5 shows snapshot plots of wave field in air-concrete half spaces. It is evident that the artificial AE source excited Rayleigh waves on the concrete surface, and as the wave propagates, the motion of surface points constantly perturbs the air at the interface, leaking vibration into the air. In addition to leaky Rayleigh waves, the direct acoustic waves propagating in the air are also observed, the acoustic velocity of air is 342 m/s calculated from the waveforms received by sensing point.

4.2.2 Measurement of the R-Wave Velocity by air-coupled MASW

Four-channel signals collected above the surface along a linear array of sensing points at equal intervals from the AE source, as shown in Fig. 4(a), are converted from offset time domain to frequency-phase-velocity domain using plane wave transformation technique, the results shown in Fig. 6 below are obtained.

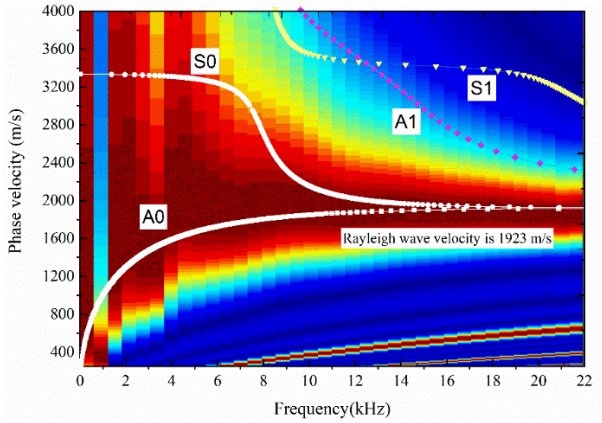

Fig. 6 Air-coupled MASW images with Lamb wave dispersion curves

Fig. 6 shows the dispersion images obtained by the air-coupled MASW. It can be seen that the dispersion curve can be extracted from the obtained MASW image. A0 and S0 modes mainly exist in the concrete slab in the low frequency region (< 10 kHz). When the frequency is greater than 12 kHz, these two modes merged together and propagated at the velocity of Rayleigh wave. The obtained leaky Rayleigh wave velocity is very consistent with that of theoretical Rayleigh wave (1923 m/s). The results demonstrate that the leaky Rayleigh wave velocity can be obtained using the air-couped MASW technique, which uses only four signals, but the image has enough resolution to determine the modal velocity clearly, and the velocity will be used for air-coupled beamforming.

4.2.3 Time-frequency analysis of leaky Rayleigh wave and Rayleigh wave

Below the corresponding position to the sensing point in air, the AE waveforms are detected at the sensing point (shown in Fig. 4(a)) on the surface of the concrete plate.

Fig. 7(a) illustrates a time domain signal obtained from one air-coupled receiver. The wave packets of leaky Rayleigh wave and direct acoustic wave can be clearly separated from each other, leaky surface wave propagates

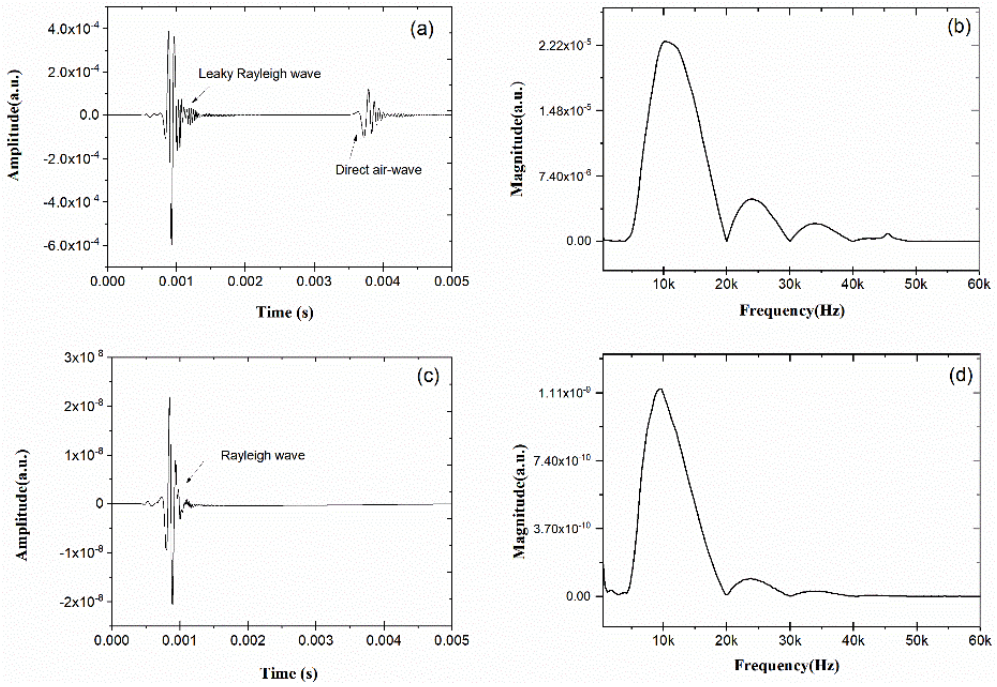

Fig. 7 Typical time domain AE signals. (a) a signal obtained in air (2 cm above concrete); (b) frequency spectrum of (a); (c) the signal at the same position as (a) is obtained on concrete surfaces; (d) frequency spectrum of (c)

faster than direct acoustic wave and has a larger amplitude. Fourier transform was performed on the first wave packet, as depicted in Fig. 7(b), the amplitude spectrum has a wide frequency range (5-20 kHz), it is consistent with the frequency range of the excitation signal, which is exactly the low frequency range we're interested in. Moreover, direct acoustic waves in this frequency range (0~20 kHz) are easily disturbed by environmental noise, so the test setup would be designed to shield the direct acoustic waves in practical application. In this study, we are only interested in leaky Rayleigh waves propagating at the air/concrete interface, and this signal is used to locate the AE source in the experiment. Fig. 7(c) is a time domain signal of Rayleigh wave received in concrete, so there are no direct acoustic waves, and the arrival time in the time domain is the same as that in Fig. 7(a), because the distance from the AE source is almost the same (the air-coupled receiver is 2 cm away from the surface). At the same time, they have the same frequency range in frequency domain. In order to save calculation time, the numerical calculations in the next section, the Rayleigh wave are used to replace the leaky Rayleigh wave in air to simulate the positioning of AE in the next section of numerical calculations.

4.3 Numerical simulation of AE source location based on a 3D solid model

A vertical impact load at the concrete surface will excite many modes of guided waves in the solid, because Rayleigh waves have larger out-of-plane motion and attenuate slower with distance than body waves (i.e., P-wave and S-wave), Rayleigh waves can travel longer distances. Fig. 8 presents the sound field screenshot of the Rayleigh wave at two different time steps. It can be observed that surface disturbances emerging from the AE source diverges in all directions. In the process of Rayleigh wave propagation, there is a large amplitude in the direction perpendicular to the plane, which disturbs the air at the interface. These disturbances are easy to be monitored by air-coupled sensors in air.

4.4 Parameter study: positioning results at different array spacing

In practice, a large number of sensors need to be arranged to monitor large civil structures, this requires each monitoring array to locate AE sources with as few sensors as possible, so as to speed up signal processing and reduce

(a) Time t1 (b) Time t2

Fig. 8 Rayleigh wave propagation at two different time steps

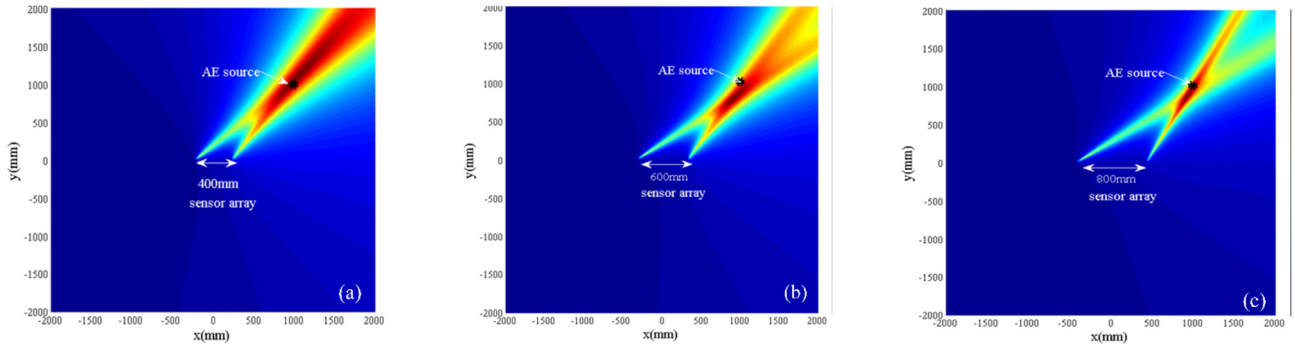

(a) 400 mm (b) 600 mm (c) 800 mm

Fig. 9 Location results of the same AE source for different array spacing

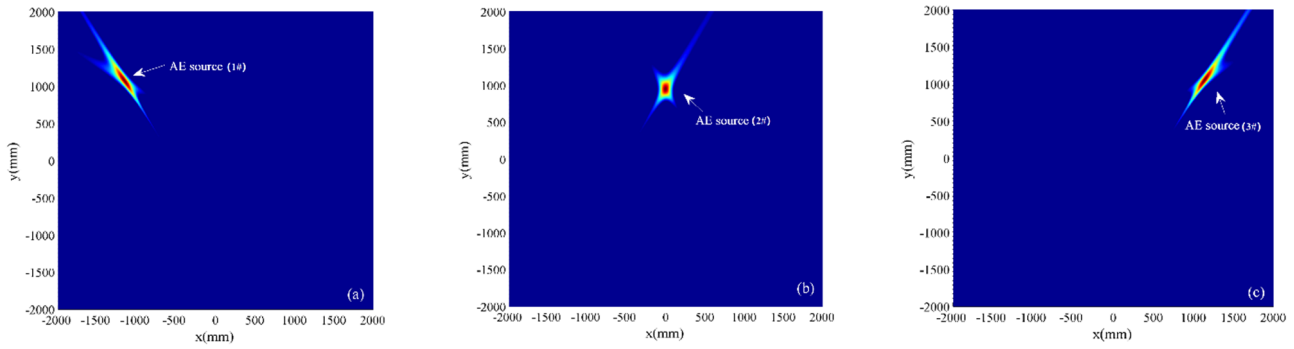

(a) AE location is (-1000,1000) mm (b) AE location is (0,1000) mm (c) AE location is (1000,1000) mm

Fig. 10 Location results of different AE sources

the cost of a single monitoring system. According to Xiao *et al*. (2014), the positioning accuracy of circular array and cross array is higher, the four-sensor square array is the simplest circular array. Therefore, four sensors are selected to form a square array in this study, the AE signals used for locating is at frequencies no greater than about 22 kHz, the array is designed to contain wavelengths down to 87 mm, a 4-sensor square planar array with a length of 60 mm was selected.

With the midpoint between two arrays as the origin, we divided the monitoring area in four quadrants. Due to the symmetry, we only study the location of acoustic emission sources in the first and second quadrants. Because the wave beam has a certain width, the cross-focusing of two wave beams are an area with large amplitude, and the coordinates corresponding to the maximum amplitude are determined as the position of the AE source. When the distance between the two arrays changes, the positioning accuracy will be affected.

If the distance is too close, the overlapping area of two wave beams becomes larger; if the distance is too large, which is not convenient for layout in practice. Therefore, optimal values for the distance between two arrays have to be studied so that the employment becomes convenient without compromising the quality of location. For this reason, a parametric study is carried out.

For distances between the two arrays, the different intervals of 200 mm, 400 mm, 600 mm, 800 mm and 1000 mm are taken for parameter research. Due to space limitations, only partial results are presented, as shown in Fig. 9. For the same AE source, as the spacing increases, the intersection region of the two beams will become smaller. For distant AE sources (e.g., 1000 mm from AE source), an interval greater than 800 mm is sufficient for accurate positioning, and an interval of 1000 mm can be used for more accurate results. For more distant AE sources from different azimuth angles, the array spacing needs to be analyzed specifically. For example, for AE sources close to the y-axis, only a relatively small spacing is required, and for AE sources close to the x-axis, a relatively large array spacing is required.

4.5 Location results of different AE source

The monitoring plane centered on the array, where AE sources are located at three different locations, the array spacing is 1000 mm, the results are shown in Fig. 10 below.

Fig. 10 shows that the actual locations of the three AE sources can be accurately located at a distance of about 1,000 mm. When the AE source is between the arrays (2# AE source), the area of beam intersection is small, so the result of positioning is most accurate among the three positions. When the AE source is in quadrant 1 (1# AE source) and quadrant 3 (3# AE source), the area of beam intersection overlaps increases, so the positioning accuracy is reduced, of course, if the AE source is on the same straight line (x-axis) as the array pair, it cannot be located (two beams are collinear). The error analysis of positioning

Table 1 Localization results of the AE source using a pair of air-coupled arrays

	Actual AE coordinates (mm)	Estimated coordinates (mm)	% of Error*
AE source (1#)	(-1000, 1000)	(-1126, 1026)	9.1%
AE source (2#)	(0, 1000)	(-1, 961)	3.9%
AE source (3#)	(1000, 1000)	(-1140, 1054)	10.6%

*Error: based on the actual AE coordinates

results is shown in Table 1, the overall position error is within 10.6 %, which can meet the monitoring requirements of large plate-like concrete structures.

From the above numerical analysis, we can draw the following conclusions:

- Loading a pulsed signal perpendicular to the plane on the surface of the concrete slab can excite a leaky Rayleigh wave at the air-concrete interface.
- The MASW data processing of four-way leaky Rayleigh wave signals can obtain dispersion images containing properties of concrete materials, such as the velocity of leaky Rayleigh wave.
- To improve the accuracy of beamforming localization, one is to reduce the beam width of a single array, and the other is to choose an appropriate distance between two arrays.
- The position of the array shall not be too close to the concrete boundary to reduce the interference from edge reflections.

These findings lead us toward the AE source localization experiments to verify this new designed system, the leaky Rayleigh wave propagating at air-concrete interface can be employed for this purpose and has unique advantages, since the Rayleigh waves have larger out-of-plane motion and attenuate slower with distance than other body wave. Also, the propagation velocity basically does not change with the increases in the propagation distance, which provides a convenient calculation condition for beamforming. Based on these investigations, the leaky Rayleigh wave will be used to carry out experimental research on location of artificial AE source.

5. Experimental verification

In this section, a comprehensive demonstration of AE source location based on leaky Rayleigh waves is carried out using an actual concrete slab. The following steps are described:

(a). Establishment of test system,
(b). MASW analysis and beamforming of leaky Rayleigh wave, and
(c). Localization of AE sources at the surface.

5.1 Experimental setup and procedure

Among all types of microphone sensors, MEMS sensors demonstrate the highest the signal to noise ratio (SNR) and sensitivity. In this study, the author purchased MEMS sensors and built the multi-sensor array monitoring system. A four-element square array and linear array (the array is a quad-microphone array expansion board for Raspberry Pi designed for AI and voice applications, Seeed company in Shenzhen, China) were selected for the test, an installation system was mounted on a straight line that allows the sensor to be placed accurately based on sensor spacing and height to the test surface. Linear array is used to conduct a MASW analysis to determine the leaky Rayleigh wave velocity, and the square array was used for beamforming.

In our study, the sensor spacing of linear array and square array is 50 mm and 60 mm respectively, and both are 20 mm height from the surface, the distance between the AE source and the first sensor is 1000 mm. A photograph of the experimental setup is illustrated in Figs. 11(a)-(b).

An artificial acoustic emission was achieved by breaking a pencil on the surface of the concrete slab (Hsu 1977). This artificial source is often used to study the characteristics of AE signal and AE source location (Sedlak *et al*. 2013). A concrete slab tested is 3000 mm long by 2000 mm wide, and has a thickness of 200 mm (P-wave velocity measured in experiments is 3444 m/s, S-wave velocity is 2109 m/s). A photograph of the experimental setup with sensor array is shown in Fig. 11. No additional treatment or preparation was performed on the concrete surface, and the tests were carried out in ambient acoustic noise conditions.

The leaky Rayleigh waves from AE source are detected by the microphones and sent to the memory card in

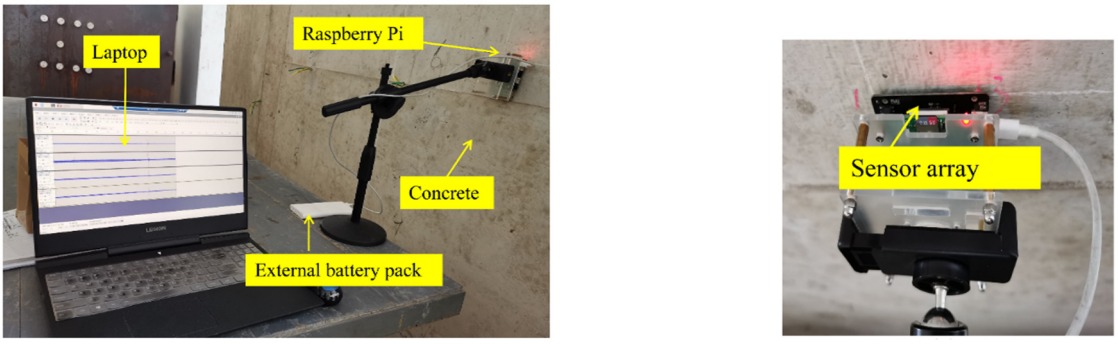

(a) Time t1 (b) Time t2

Fig. 11 The air-coupled experimental setup

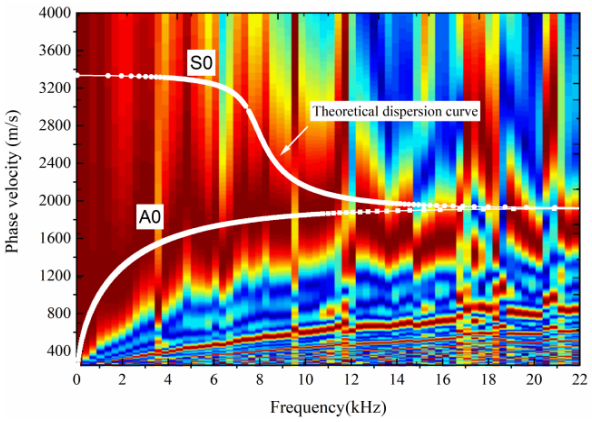

Fig. 12 Air-coupled MASW images with Lamb wave dispersion curves. Experimentally obtained dispersion images of concrete slab (Theoretical dispersion curve was calculated using the measured parameters)

Table 2 Localization results of the AE source on the plate-like concrete using air-coupled arrays

AE source	Actual location (cm)	Estimated location (cm)	% of Error*
1#	(-50, 100)	(-39,90)	13.3%
2#	(0, 100)	(9,104)	9.8%
3#	(50, 100)	(50,80)	17.8%

*Error: based on the actual AE coordinates

Raspberry Pi. Each continuous-time signal was to be sampled and stored for duration of 10 ms at a frequency resolution of about 50 Hz and a sampling frequency of 96 kHz. The test data are transferred to a personal laptop using Raspberry Pi to transmit data wirelessly for storage and further analysis.

5.2 MASW analyses

Fig. 12 shows the dispersion images obtained by the linear MEMS array which is parallel to the direction of wave propagation from a concrete slab. Like the dispersion image obtained by numerical analysis, it is also obtained by MASW processing of four signals, but the dispersion image here is not so pure (this is due to concrete's effect on the frequency content of AE signals.), but it is sufficient to detect that the Rayleigh wave has a pulse group velocity of 1922 m/s, which agrees very well with the theoretical analysis (the same concrete material parameters are used for theoretical analysis and numerical study, the predicted dispersion image is shown in Fig. 6). The leaky Rayleigh wave velocity extracted from the dispersion image will be used for beamforming data processing.

5.3 Experimental results of AE source localization

As observed in Fig. 13, the AE source 1# located about 110 cm away from the arrays was located by the beamforming array. For all three artificial AE source, the location results are summarized in Table 2.

Based on the analysis of the positioning results, the conclusion is dawn that the location of the AE source can be achieved by an air-coupled monitoring system. AE source 1# and AE source 3# are in the first and second quadrants of the monitoring plane respectively, and AE source 2# is on a straight line perpendicular to the array connecting line, For the monitoring plane determined by the square array pair, these three positions represent all possible incoming wave directions (except the AE source on the line (x-axis) where the array pair is located). Unlike the traditional located sound source, which needs to be surrounded by sensors, the monitoring system in this study monitors a circular planar area determined by the monitoring unit. For single-array pair positioning, the error between estimated and true location is less than 17.8% in the range of approximately 110 cm, the error is within the theoretical prediction range. If multiple array pairs are used together, a larger area can be monitored, this accuracy is sufficient for most field monitoring applications. For multiple AE source localization over longer distances, a larger concrete slab will be produced for testing in the future.

6. Discussions

For thick, plate-like concrete structures, when structural damage occurs, Rayleigh waves propagate at the solid interface and have larger out-of-plane motion and attenuate slower with distance than body waves. The MEMS air-coupled sensor can make full use of the advantage of AE technique which can detect active defects, and it is convenient to be applied to the damage monitoring of practical large-scale civil structures.

The test results of concrete slab show that the location of the AE source can be achieved by an air-coupled MEMS array pair, The deviation mainly comes from the inaccuracy of the position of the artificial AE source, and the AE signal with low frequency is used in this study, and its wavelength is long (about 12 cm), which determines the positioning accuracy of this method.

There are also some limitations for beamforming arrays pairs. First, the cross-beam imaging location based on array pairs is not accurate for locating the AE source near the *x*-axis. In addition, since beamforming depends on the comparison of signal waveforms, it is very important that all sensors in the array have the same amplitude and phase response, this requires a high consistency of the four MEMS sensors in an array. Another aspect not considered in the study is the effect of ambient noise on beamforming localization. In the next step, the artificial AE source will be replaced by the actual concrete fracture test, the single array positioning method based on polar coordinates will be studied, which can locate the AE source in a 2D plane with a 360-degree sweep.

7. Conclusions

This article presents a non-contact (air-coupled) AE

localization method for plate-like concrete structures. Considering the challenges and problems faced by air-coupled sensors in monitoring concrete structures, this preliminary study is of great significance for the development of new health monitoring system for large civil structures. Numerical simulations and experiments were conducted to evaluate the performance of the proposed method. Based on the above results, the following conclusions were drawn:

- A wireless air-coupled monitoring system for the localization of AE sources was developed, based on air-coupled MASW and beamforming, the locations of artificial AE sources are detected in air over a long distance (more than 1m) from the concrete slab surface in the low frequency range of 0-22 kHz. The error between estimated and true location is less than 17.8% in the range of approximately 110 cm, the error is within the theoretical prediction range.
- In the simulation, the propagation characteristics of leaky Rayleigh wave were carried out by employing a time-domain based finite element method model. The findings showed that the dispersion properties of leaky Rayleigh wave agreed well with Lamb wave dispersion curves.
- In the experiment, the microphone sensors are installed on the Raspberry Pi to form a wireless connected monitoring unit, which was able to monitor and analyze data to obtain the position of AE source independently, when the more units are combined, the more accurate AE source can be located.
- AE source in thick plate-like concrete structures can be located by the proposed system with an acceptable accuracy, and each array has only four microphones, considering the low cost of each microphone and convenient installation, the non-contact array provides a potential monitoring method for the health of the entire large civil engineering structure.

Acknowledgments

This work was supported by the National Natural Science Foundation of China (No. 41877219 and 12274463); Chongqing Research Program of Basic Research and Frontier Technology (No. cstc2015jcyjBX0073); Natural Science Foundation of Chongqing (No. cstc2019jcyj msxmX0585); Chongqing Graduate Student Research Innovation Project (No. CYB21248); and the Scientific and Technological Research Program of Chongqing Municipal Education Commission (KJQN202012901).

References

Aggelis, D.G. and Matikas, T.E. (2012), "Effect of plate wave dispersion on the acoustic emission parameters in metals", *Comput. Struct.*, **98-99**, 17-22. https://doi.org/10.1016/j.compstruc.2012.01.014

Banjara, N.K., Sasmal, S. and Srinivas, V. (2019), "Damage progression study in fibre reinforced concrete using acoustic emission technique", *Smart Struct. Syst., Int. J.*, **23**(2), 173-184. https://doi.org/10.12989/sss.2019.23.2.173

Carpinteri, A., Lacidogna, G., Corrado, M. and Battista, E.D. (2016), "Cracking and crackling in concrete-like materials: A dynamic energy balance", *Eng. Fract. Mech.*, **155**, 130-144. https://doi.org/10.1016/j.engfracmech.2016.01.013

Chen, J., Wu, Y. and Yang, C. (2019), "Damage assessment of concrete using a non-contact nonlinear wave modulation technique", *NDT & E International*, **106**(SEP.), 1-9. https://doi.org/10.1016/j.ndteint.2019.05.004

Du, F., Li, D.S. and Qiu, D. (2021), "Cluster analysis and damage identification for FRP/steel-confined RC column using AE technique", *Smart Struct. Syst., Int. J.*, **27**(3), 407-419. https://doi.org/10.12989/sss.2021.27.3.407

Ferguson, B.G., Criswick, L.G. and Lo, K.W. (2002), "Locating far-field impulsive sound sources in air by triangulation", *J. Acoust. Soc. Am.*, **111**(1), 104-116. https://doi.org/10.1121/1.1402618

Hsu, N.N. (1977), Acoustic emissions simulator, US Patent; US4018084.

Kaczmarek, M., Piwakowski, B. and Drelich, R. (2017), "Noncontact ultrasonic nondestructive techniques: state of the art and their use in civil engineering", *J. Infrastr. Syst.*, **23**(1), B4016003. https://doi.org/10.1061/(ASCE)IS.1943-555X.0000312

Kuang, K.S.C., Li, D. and Koh, C.G. (2016), "Acoustic emission source location and noise cancellation for crack detection in rail head", *Smart Struct. Syst., Int. J.*, **18**(5), 1063-1085. https://doi.org/10.12989/sss.2016.18.5.1063

Li, D., Shao, J., Ou, J. and Wang, Y. (2017), "Damage analysis of carbon nanofiber modified flax fiber composite by acoustic emission", *Smart Struct. Syst., Int. J.*, **19**(2), 127-136. https://doi.org/10.12989/sss.2017.19.2.127

McLaskey, G.C., Glaser, S.D. and Grosse, C.U. (2010), "Beamforming array techniques for acoustic emission monitoring of large concrete structures", *J. Sound Vib.*, **329**(12), 2384-2394. https://doi.org/10.1016/j.jsv.2009.08.037

Ongpeng, J.M.C., Oreta, A.W.C. and Hirose, S. (2018), "Contact and noncontact ultrasonic nondestructive test in reinforced concrete beam", *Adv. Civil Eng.*, **2018**, 5783175. https://doi.org/10.1155/2018/5783175

Park, C.B., Miller, R.D. and Xia, J. (1998), "Imaging dispersion curves of surface waves on multi-channel record", SEG Technical Program Expanded Abstracts 1998, 1377-1380. https://doi.org/10.1190/1.1820161

Plona, T.J., Mayer, W.G. and Behravesh, M. (1975), "Rayleigh and Lamb waves at liquid-solid boundaries", *Ultrasonics*, **13**(4), 171-175. https://doi.org/10.1016/0041-624X(75)90086-4

Qiu, Q. and Lau, D. (2021), "Defect detection of FRP-bonded civil structures under vehicle-induced airborne noise", *Mech. Syst. Signal Process.*, **146**, 106992. https://doi.org/10.1016/j.ymssp.2020.106992

Redwood, M. (1967), "Rayleigh and Lamb waves", *Ultrasonics*, **5**(4), 260-260. https://doi.org/10.1016/0041-624X(67)90079-0

Sedlak, P., Hirose, Y. and Enoki, M. (2013), "Acoustic emission localization in thin multi-layer plates using first-arrival determination", *Mech. Syst. Signal Process.*, **36**(2), 636-649. https://doi.org/10.1016/j.ymssp.2012.11.008

Shahidan, S., Pulin, R., Bunnori, N.M. and Holford, K.M. (2013), "Damage classification in reinforced concrete beam by acoustic emission signal analysis", *Constr. Build. Mater.*, **45**, 78-86. https://doi.org/10.1016/j.conbuildmat.2013.03.095

Wang, X., Liu, X., He, T., Tai, J. and Shan, Y. (2020), "A novel joint localization method for acoustic emission source based on

time difference of arrival and beamforming", *Appl*. *Sci*., **10**(22), 8045. https://doi.org/10.3390/app10228045

Xiao, D., He, T., Pan, Q., Liu, X., Wang, J. and Shan, Y. (2014), "A novel acoustic emission beamforming method with two uniform linear arrays on plate-like structures", *Ultrasonics*, **54**(2), 737-745. https://doi.org/10.1016/j.ultras.2013.09.020

FC